

Experimental investigation of electron transport properties of gallium nitride nanowires

Abhishek Motayed,^{1,a)} Albert V. Davydov,¹ S. N. Mohammad,² and John Melngailis³

¹National Institute of Standards and Technology, Gaithersburg, Maryland 20899, USA

²Department of Materials Science and Engineering, University of Maryland, College Park, Maryland 20742, USA

³Department of Electrical and Computer Engineering, University of Maryland, College Park, Maryland 20742, USA

(Received 24 February 2008; accepted 30 April 2008; published online 16 July 2008)

We report transport properties of gallium nitride (GaN) nanowires grown using direct reaction of ammonia and gallium vapor. Reliable devices, such as four-terminal resistivity measuring structures and field-effect transistors, were realized by dielectrophoretically aligning the nanowires on an oxidized silicon substrate and subsequently applying standard microfabrication techniques. Room-temperature resistivity in the range of $(1.0\text{--}6.2)\times 10^{-2}\ \Omega\ \text{cm}$ was obtained for the nanowires with diameters ranging from 200 to 90 nm. Temperature-dependent resistivity and mobility measurements indicated the possible sources for the *n*-type conductivity and high background charge carrier concentration in these nanowires. Specific contact resistance in the range of $5.0\times 10^{-5}\ \Omega\ \text{cm}^2$ was extracted for Ti/Al/Ti/Au metal contacts to GaN nanowires. Significant reduction in the activation energy of the dopants at low temperatures ($<200\ \text{K}$) was observed in the temperature-dependent resistivity measurement of these nanowires, which is linked to the onset of degeneracy. Temperature-dependent field-effect mobility measurements indicated that the ionized impurity scattering is the dominant mechanism in these nanowires at all temperatures. © 2008 American Institute of Physics. [DOI: 10.1063/1.2952035]

I. INTRODUCTION

Semiconducting nanowires have drawn tremendous interest largely because unlike their metallic counterparts they provide means for controlling their electronic properties through dopant control, band-gap engineering, and heterostructure formation. This has resulted in numerous device applications ranging from field-effect transistors (FETs),¹ single nanowire light-emitting diodes,² lasers,³ photodetectors,⁴ photovoltaic cell,⁵ to chemical/biological sensors.⁶ Although these impressive results demonstrate the viability of the nanowire devices as basic building blocks for complex systems, the growth methods still lack consistency and theoretical understanding.^{7,8} It is a well-known fact that the nanowires grown using most of the available methods today have unusually high background charge carrier concentrations, which may result from point defects (impurities and vacancies)⁹ and/or extended line defects.¹⁰ In order to realize high-performance nanowire devices it is important to know exactly how these defects interact with the charge carriers in these nanostructures. Unfortunately, few reports on the fundamental transport properties in semiconducting nanowires^{11–14} have been published so far.

Determining intrinsic properties such as resistivity and carrier mobility of semiconducting nanowires accurately is important as it enables us to estimate important device parameters. Figure 1 is the schematic representation of the four-terminal (4T) structure usually used to measure resistivity of nanowires. Current (I_{12}) is forced between the outer

two pads (1 and 2) and the voltage drop (V_{34}) is measured between the inner two pads (3 and 4). The resistivity (ρ) for the nanowire can simply be calculated using the relationship $\rho=(V_{34}/I_{12})\pi r^2/l$, where r is the radius of the nanowire and l is the length of the nanowire between the inner two contacts. This geometry ensures that the contact resistances are not included in the intrinsic material resistance. Utilizing this structure we can estimate different material properties such as (a) intrinsic resistivity (ρ), (b) contact resistance of the metal-nanowire junction, and (c) temperature-dependent resistivity, which could provide the activation energy of the dopants. Both carrier concentration (n) and mobility (μ) could also be determined from the electrical characteristics of FETs, and using the relationship $\rho=1/q\mu n$ one can independently calculate the carrier concentration or mobility from the resistivity measurements.

In this paper we have presented the temperature-dependent resistivity and mobility measurements of GaN

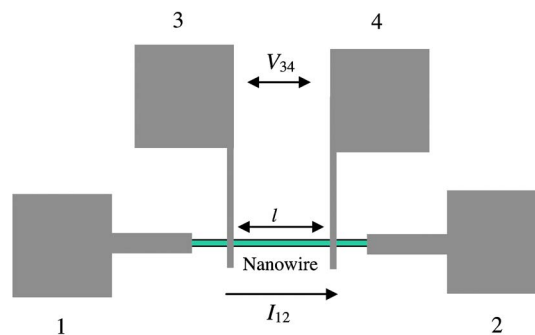


FIG. 1. (Color online) Schematic representation of 4T structure used for resistivity measurement of nanowires. A small current is forced between pads 1 and 2, and corresponding voltage drop is measured between pads 3 and 4.

^{a)}Author to whom correspondence should be addressed. Electronic mail: amotayed@nist.gov.

nanowires, and established that the ionized impurity scattering mechanism is the dominant process in these nanostructures even at room temperatures. The weak temperature dependence of the resistivity at lower temperatures ($T < 200$ K) could be explained by the reduction in the activation energy of the donors at temperatures below 200 K due to the onset of degeneracy.

II. EXPERIMENTAL PROCEDURE

Gallium nitride nanowires with diameters ranging from 50 to 250 nm and lengths up to 200 μm were grown by direct reaction of gallium vapor with flowing ammonia at 850–900 $^\circ\text{C}$ in a horizontal furnace.¹⁵ Electron backscattered diffraction and transmission electron microscopy confirmed that the growth direction of the nanowires is along the a -axis of the wurtzite structure.¹⁰ A suspension of the nanowires in isopropanol, formed by sonicating the growth matrix, was dispersed on a 600 nm (thermally grown) SiO_2/Si (p -type, $\rho=0.01$ Ω cm) substrate with Ti (30 nm) metal pads. Alignment of the nanowires was obtained by applying 20 V peak-to-peak sinusoidal voltage at 1 kHz between the metal pads. Details of the alignment procedure was described elsewhere.¹⁰ Alignment of the nanowires was followed by the deposition of a 50 nm SiO_2 passivation layer using plasma enhanced chemical vapor deposition (CVD). The oxide was removed over the metal-nanowire contact area and a second metal layer (Ti/Al/Ti/Au—30/100/30/30 nm) was deposited.¹⁰ Annealing of the complete device structures at 650 $^\circ\text{C}$ for 30 s in argon was performed to obtain Ohmic contacts. Room-temperature device measurements were performed in a standard probe station in air whereas low-temperature measurements were performed in an open-cycle cryogenic probe station. After completion of the electrical measurements, field-emission scanning electron microscope (FESEM) was used to study the morphology of the nanowires and to measure the dimensions of the nanowires.

III. RESULTS AND DISCUSSIONS

The FESEM image of a 4T structure is shown in the inset of Fig. 2. The diameter of this nanowire was 132 nm and the length between the inner two pads was 8.9 μm . In Fig. 2 the two-terminal (2T) and 4T current-voltage (I - V) characteristics are shown together, where the effect of contact resistance is visible. The linear I - V characteristics indicate the Ohmic nature of the contacts. The 2T I - V characteristics for this nanowire was measured utilizing the inner two contacts, whereas 4T I - V plot was obtained by varying the current through the outer contacts and measuring the respective voltage drops between the inner two contacts. For resistivity measurement a small current (100 nA) was used to minimize the joule heating of the nanowire. Measurement using the above mentioned procedure on several different nanowires with diameters ranging from 200 to 90 nm yielded resistivity in the range of $(1.0\text{--}6.2) \times 10^{-2}$ Ω cm, with 20% variation in the resistivity for nanowires with similar diameters. We will later discuss the possible origin of such low resistivity values in these unintentionally doped nanowires. The contact resistance (R_c) can be computed using the relationship $R_c = (R_{2T} - R_{4T})/2$, where R_{2T} and R_{4T} are the 2T and

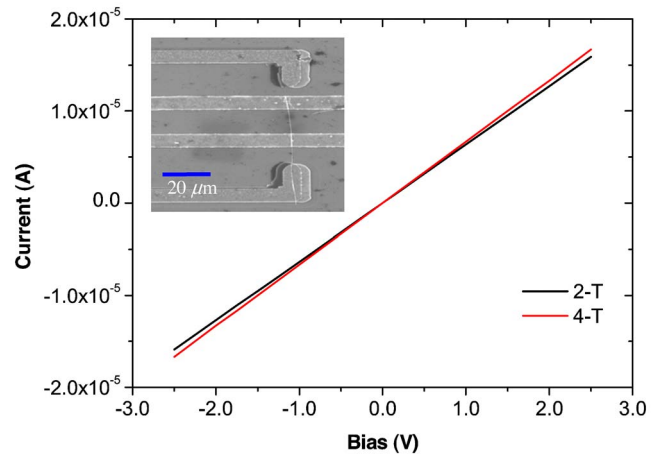


FIG. 2. (Color online) 2T and 4T I - V characteristics of a nanowire (shown in the inset) with diameter of 132 nm and length of 8.9 μm . Black curve corresponds to the 2T measurement, where I - V measurement is taken using the inner two contacts. Red curve corresponds to the 4T measurement, where different currents are forced through the outer two contacts and corresponding voltage drops are measured between the inner two contacts and plotted inversely. (Inset) FESEM image of a nanowire with four metal contacts.

4T resistances, respectively, which are the inverse of the slopes of the 2T and 4T curves. For the nanowire shown in the inset of Fig. 2, the contact resistance calculated was approximately 240 k Ω . The specific contact resistance (ρ_c) can be calculated using the relationship $\rho_c = R_c \times A$, where A is the nanowire-metal contact area. As these devices have both top and bottom metal contacts, the metal-nanowire contact area is essentially $2\pi r \times l_c$, where r is the radius of the nanowire and l_c is the metal contact length covering the nanowire. The specific contact resistances for ten different nanowires were in the range of $(2.0\text{--}5.0) \times 10^{-5}$ Ω cm². Specific contact resistance of Ti/Al/Ti/Au contacts to the n -type GaN thin films ($N_D = 5 \times 10^{17}$ cm⁻³) annealed at 750 $^\circ\text{C}$, is in the range of 3.0×10^{-6} Ω cm².¹⁶ The higher specific contact resistances for the contacts to the GaN nanowires could be due to the lower annealing temperature used than for the metal contacts to thin films.

Using the inner two contacts as the source (S) and drain (D) electrodes and the Si substrate as the back gate, nanowire channel current (I_{DS}) can be modulated by applying a bias (V_{GS}) to the Si substrate. Depletion mode behavior with the n -type conduction is observed for all of the devices, which is often attributed to the presence of lattice defects, and impurities such as oxygen.¹² The electron field-effect mobility (μ) is calculated using the relationship¹⁰

$$\mu = \frac{g_m}{V_{DS}} \frac{l \ln\left(\frac{4t_{ox}}{d}\right)}{2\pi\epsilon_0\epsilon_{\text{SiO}_2}}, \quad (1)$$

where transconductance (g_m) is the slope $\partial I_{DS}/\partial V_{GS}$ of the I_{DS} versus the V_{GS} plot measured at $V_{GS}=0$ V and drain-source voltage $V_{DS}=1$ V, l and d are the length and diameter of the nanowire, respectively, t_{ox} is the oxide thickness (600 nm), ϵ_0 is the permittivity of free space, and ϵ_{SiO_2} is the permittivity of silicon dioxide. Room-temperature mobility calculated using Eq. (1) for the nanowire shown in the inset

TABLE I. Comparison of the GaN nanowire material parameters measured by various other researchers with the present work. (Nanowires grown by all the methods described here are unintentionally doped.)

Growth method	Diameter range (nm)	Metal contact	Resistivity (Ω cm)	Mobility ($\text{cm}^2 \text{V}^{-1} \text{s}^{-1}$)	Carrier concentration (cm^{-3})	Ref.
Laser-assisted catalytic growth using Fe catalyst	10	Ti/Au (50/70 nm)	...	150–650	10^{18} – 10^{19}	17
CVD using Ni catalyst	30–70	Ti/Au (20/50 nm)	...	2.15	...	18
Hot-wall CVD with different catalysts	25–200	Ni/Au (50/200nm)	...	10–30	10^{20} – 10^{19}	9
CVD with Au/Pd catalyst	66–184	Pt (100nm)	0.01	...	2.3×10^{19}	12
CVD with Ni catalyst	20–40	Ti/Al/Mo/Au	...	17.5	1.44×10^{19}	19
CVD with Ni catalyst	35–120	Ti/Au (30/120 nm)	...	30	2×10^{17}	20
Direct reaction of NH_3 and Ga	90–200	Ti/ Al/ Ti/Au (30/100/ 30/30nm)	0.01–0.062	60–300	2×10^{18}	Present work

of Fig. 2 was $65 \text{ cm}^2 \text{V}^{-1} \text{s}^{-1}$. Variation in the electron mobility with nanowire diameter has been reported earlier.¹⁰ Using the measured resistivity and mobility, one can independently calculate the carrier concentration for this nanowire using $n=1/(q\mu\rho)$, which was about $3.5 \times 10^{18} \text{ cm}^{-3}$. The equilibrium carrier concentration (n) can also be calculated from the threshold voltage (V_{th})

$$n = \frac{\epsilon_0 \epsilon_{\text{SiO}_2} V_{\text{th}}}{qr^2 \ln\left(\frac{4t_{\text{ox}}}{d}\right)}, \quad (2)$$

where V_{th} is the threshold voltage, q is electronic charge, and r is the radius of the nanowire. Although this particular device did not exhibit complete channel depletion, other smaller diameter nanowires from the same growth run showed complete pinch off with V_{th} in the range of -20 to -30 V. Electron concentration calculated using Eq. (2) for these nanowires were in the range of $2.0 \times 10^{18} \text{ cm}^{-3}$.¹⁰ As it is evident this value is remarkably close to the value obtained from the resistivity calculation. Table I summarizes relevant material properties of GaN nanowires measured by various groups. It is clear that existing growth methods generally result in very high n -type background carrier concentration.

Temperature-dependent resistivity measurement is an important tool in determining donor/acceptor ionization energies in a semiconductor. From such measurements we could infer the nature of the dopant species. The data provided in Table I establish the need for such measurement in revealing the source of high background concentration in GaN nanowires. So far the reports of temperature-dependent resistance measurements carried out on GaN nanowires are obtained by 2T methods.^{12,20–22} High contact resistances and temperature-dependent contact properties due to thermionic emission in the metal-nanowire junction make analyzing the results difficult. We measured 4T resistivity of GaN nanowires from 290 down to 70 K. Figure 3(a) shows the resistivity as a function of the temperature for the nanowire shown in Fig. 2 (inset). Although resistivity data are shown for one nanowire, very similar trend has been observed for a large number of devices. It is clear that the resistivity is weakly dependent on the temperature for these nanowires. The resistivity variation is noticeably smaller at temperatures below 200 K. The temperature-dependent resistivity clearly

does not fit the simple thermal activation energy model. Other groups also observed this type of weak and variable dependence of the resistance on the temperature for GaN nanowires.^{12,20,21} Although different conduction mechanisms such as variable-range hopping,¹² fluctuation-dominated tunneling,²⁰ and impurity band conduction²¹ have been proposed to explain the results, no attempt has been made to

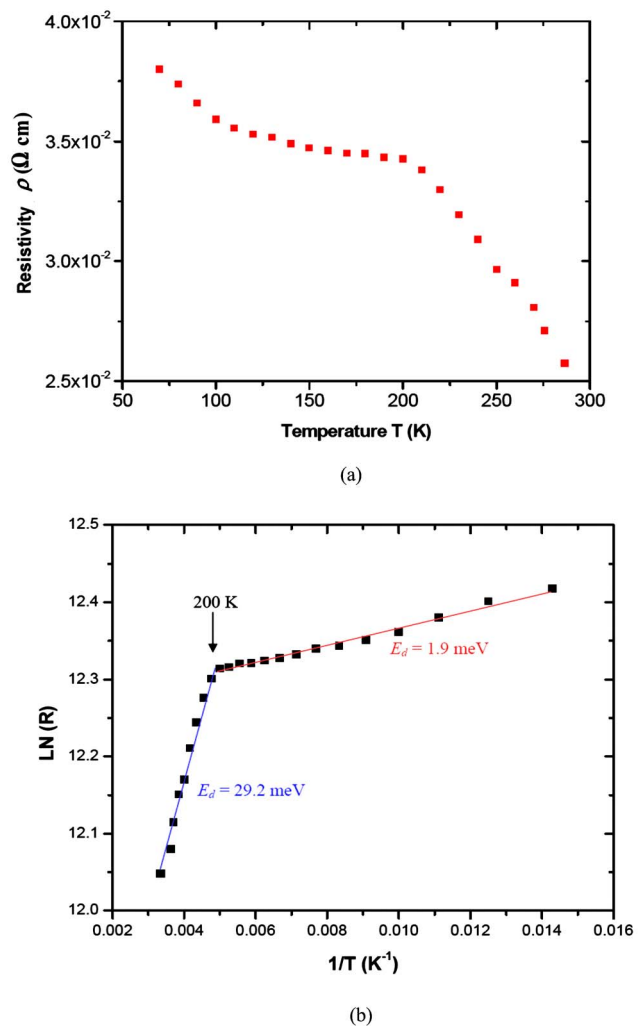


FIG. 3. (Color online) (a) Temperature-dependent resistivity measurement for the nanowire shown in Fig. 2 (inset). (b) Activation energy plot [$\ln(R)$ vs $1/T$] showing the two different activation energy regimes. Red curve is the linear fit for $200 \text{ K} \leq T < 300 \text{ K}$ with $E_d = 29.2 \text{ meV}$ and blue curve is the linear fit for $70 \text{ K} < T < 200 \text{ K}$ with $e E_d = 1.9 \text{ meV}$.

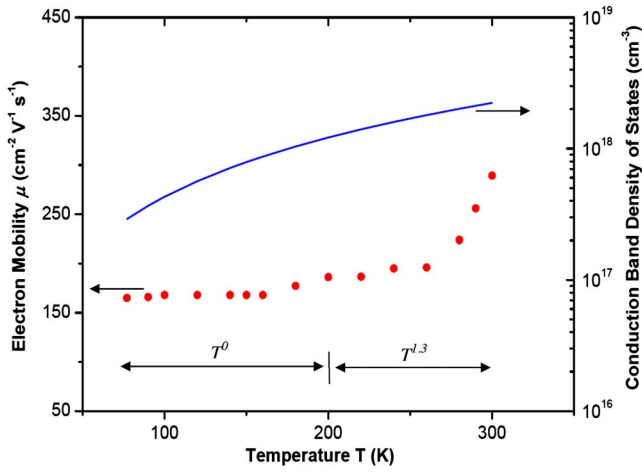


FIG. 4. (Color online) Field-effect electron mobility of a 200 nm diameter nanowires as a function of temperature is shown in the right hand axis (red dots). Calculated conduction band density of states is plotted with the right hand axis (blue line).

correlate the material properties (e.g., dopant ionization energy and carrier concentration) to the experimental observations. As these nanowires are uncompensated and the donor concentration is much higher than the intrinsic electron concentration, the equilibrium electron concentration (n) is related to the donor activation energy E_d ($E_d = E_C - E_D$, where E_C and E_D are conduction band minimum and donor energy level, respectively) by

$$n \cong \frac{1}{\sqrt{2}} \sqrt{(N_D N_C)} \exp(-E_d/2k_B T). \quad (3)$$

Substituting for n in the relationship $\rho = 1/\mu q n$, we obtain

$$\rho \cong \frac{1}{\mu q} \sqrt{\frac{2}{(N_D N_C)}} \exp(E_d/2k_B T). \quad (4)$$

The N_D and N_C are the donor concentration and conduction band density of states, respectively, k_B is Boltzmann's constant, and T is the absolute temperature. Figure 3(b) is the Arrhenius plot of the 4T resistance in the temperature range of 290–70 K. Two distinct slopes with two different activation energies ($E_d = 29.2$ meV for $200 \text{ K} \leq T < 300 \text{ K}$ and $E_d = 1.9$ meV for $70 \text{ K} < T < 200 \text{ K}$) can be seen in the plot. Unintentionally doped GaN thin films are always n -type, with nitrogen vacancies and other structural defects such as dislocations acting as shallow donors. Both oxygen and nitrogen vacancies are shallow donors in GaN with ionization energies of 29 (Ref. 23) and 30 meV,²⁴ respectively. The activation energy E_d value in the temperature range of 290–200 K suggests that oxygen and/or nitrogen vacancies might be responsible for the background concentration. The weak temperature dependence of the resistivity below 200 K with activation energy of 1.9 meV indicates that a different conduction mechanism is dominant below 200 K.

In order to understand the scattering mechanism dominating the conduction in these nanowires, temperature-dependent mobility measurements were performed. Plot of the field-effect mobility of a 200 nm diameter nanowire as function of temperature is shown in Fig. 4. In thin film enhancement mode metal-oxide-semiconductor FETs, the field-

effect mobility is always smaller than the drift mobility, as the charge conduction takes place at the oxide-semiconductor interface region, where scattering is usually enhanced. Due to high carrier concentrations in these nanowires, the majority of the channel conduction occurs in the undepleted portion of the nanowire; hence the field-effect mobility is the drift mobility in these nanowires. In high quality nondegenerate GaN thin films and bulk crystals, mobility is dominated mainly by polar optical phonon, piezoelectric acoustic phonon, and ionized impurity scattering at high, moderate, and low temperatures, respectively.²⁵ Electron mobility initially increases with decreasing temperature as the phonon scattering is minimized and the transition to ionized impurity dominated scattering is accompanied by a maximum in the mobility curve. For lower temperatures, the mobility has a $T^{3/2}$ temperature dependence, which signifies ionized impurity scattering. However, in these nanowires, we did not observe a regime where mobility increased with decreasing temperature. This could indicate that the ionized impurity scattering is the dominant process in the studied temperature range. The observed trend could be qualitatively understood by the Brooks–Herring (BH) theory of ionized impurity scattering, which predicts the mobility for²⁶

(a) nondegenerate statistics

$$\mu = \frac{128 \sqrt{2} \pi \epsilon^2 (k_B T)^{3/2}}{N_I Z^2 q^3 m^{*1/2} [\ln(1+y) - y/(1+y)]}, \quad (5a)$$

where

$$y = \frac{24 \epsilon m^* (k_B T)^2}{\hbar^2 q^2 n}, \quad (5b)$$

(b) degenerate statistics

$$\mu = \frac{24 \pi^3 \epsilon^2 \hbar^3 n}{N_I Z^2 q^3 m^{*2} [\ln(1+y) - y/(1+y)]}, \quad (6a)$$

where

$$y = \frac{3^{1/3} 4 \pi^{8/3} \epsilon \hbar^2 n^{1/3}}{q^2 m^*}. \quad (6b)$$

In the above equations ϵ is the permittivity of GaN, N_I is the ionized impurity concentration, Z is the integral ionic charge, m^* is the effective mass of electron in GaN, n is the electron concentration, and \hbar is the reduced Planck's constant. If one neglects the intrinsic dependences of n and N_I on the temperature, it is clear that this theory predicts $T^{3/2}$ and T^0 dependences of the mobility for asymptotically nondegenerate and degenerate distributions, respectively. Experimentally observed trend is remarkably close to what was predicted by the BH theory. The measured mobility has a $T^{1.3}$ dependence from room temperature down to 200 K, after which it remains invariant with the temperature (Fig. 4). The transition temperature of 200 K between the two regimes ($T^{1.3}$ and T^0) could be explained by the onset of degeneracy in these nanowires. The conduction band density of states in GaN has a temperature dependence of [Fig. 4.(blue curve)]

$$N_C \cong 4.3 \times 10^{14} T^{3/2} (\text{cm}^{-3}). \quad (7)$$

As one can infer from Fig. 3, the carrier concentration for these nanowires has weak temperature dependence. For

GaN, at 300 K, the effective density of states in the conduction band is $2.23 \times 10^{18} \text{ cm}^{-3}$, and around 200 K, it drops to about $1.2 \times 10^{18} \text{ cm}^{-3}$. Carrier concentration for these GaN nanowires is in the range of $2.0 \times 10^{18} \text{ cm}^{-3}$, and considering it is invariant with the temperature, degeneracy can occur around 200 K in these nanowires. Exact determination of the transition temperature, at which the degeneracy sets in, would require a precise determination of the carrier concentration, which is often challenging for nanowires. Similar temperature-dependent behavior of the field-effect electron mobility has been reported in Mn-doped ZnO nanowires.¹⁴

In both temperature-dependent resistivity and mobility measurements we observed a change in the nature of the temperature dependence around 200 K [see Figs. 3(b) and 4]. The weak temperature dependence of the resistivity below 200 K with activation energy of 1.9 meV would indicate that the ionization energy of the dopants is negligible at these temperatures. Impurities in semiconductors are generally represented as a localized level at a fixed energy with respect to the valence or conduction bands. This model breaks down when impurity concentration approaches the conduction band or valence band density of states. It is a well-known observation in other semiconductors that the ionization energy decreases with increasing impurity concentration.²⁷ The ionization energy goes to zero at the impurity concentration where metallic impurity conduction occurs, which is the Mott transition for semiconductors. This transition has been predicted to occur when the ratio of average separation r of the impurity atoms to the radius of the hydrogenlike impurity a^* is about 3,²⁷

$$r/a^* \approx 3.0, \quad (8)$$

where r and a^* are given by the relations

$$r = \left(\frac{3}{4\pi N} \right)^{1/3}, \quad a^* = \left(\frac{\epsilon_s}{\epsilon_0} \right) \left(\frac{m_0}{m^*} \right) 0.5 \times 10^{-8} \text{ cm}. \quad (9)$$

N is the dopant concentration, ϵ_s and ϵ_0 are the dielectric permittivity of semiconductor and vacuum respectively, and m_0 and m^* are the free electron mass and electron effective mass in the semiconductor, respectively. For GaN with $\epsilon_s/\epsilon_0=8.9$ and $m^*/m_0=0.22$, the dopant concentration N which satisfies the Eq. (8) is about $1.0 \times 10^{18} \text{ cm}^{-3}$. A low value of activation energy at low temperatures is an indication that a Mott's transition has occurred with the formation of an impurity band and the conduction is occurring through that band.²⁸

IV. CONCLUSION

Detailed transport measurements have been done on unintentionally doped n -type GaN nanowires grown using direct reaction of NH_3 and Ga. Temperature-dependent resistivity measurements indicated that the observed high background concentration in these nanowires possibly originate from oxygen impurities or nitrogen vacancies, with thermal activation of dopants determining the carrier concentrations in the range of 290–200 K. Measured activation energy of the resistivity in this temperature range matched closely to the ionization energies of both O impurity and N vacancy.

Temperature-dependent mobility measurements revealed that the ionized impurity scattering dominated the transport through these nanowires. The onset of degeneracy in the nanowire is marked by the change in the temperature dependence of electron mobility from $T^{1.3}$ to T^0 .

ACKNOWLEDGMENTS

Authors would like to thank Dr. M. He of Howard University for providing the GaN nanowire samples used in this study. The nanowire devices were fabricated at the Nanofab clean room of the NIST Center for Nanoscale Science and Technology. We thank Norman Sanford and Kristine Bertness of NIST for helpful discussion. This work was supported by ARO/DTRA contract no. W911-NF-06-1-0464.

- ¹Y. Cui, X. Duan, J. Hu, and C. M. Lieber, *J. Phys. Chem. B* **104**, 5213 (2000).
- ²F. Qian, Y. Li, S. Gradečak, D. Wang, C. J. Berrelet, and C. M. Lieber, *Nano Lett.* **4**, 1975 (2004).
- ³X. Duan, Y. Huang, R. Agarwal, and C. M. Lieber, *Nature (London)* **421**, 241 (2003).
- ⁴H. Kind, H. Yan, B. Messer, M. Law, and P. Yang, *Adv. Math.* **14**, 158 (2002).
- ⁵B. Tian, X. Zheng, T. J. Kempa, Y. Fang, N. Yu, G. Yu, J. Huang, and C. M. Lieber, *Nature (London)* **449**, 885 (2007).
- ⁶G. Zheng, F. Patolsky, Y. Cui, W. U. Wang, and C. M. Lieber, *Nat. Biotechnol.* **23**, 1294 (2005).
- ⁷K. A. Dick, K. Deppert, L. S. Karlsson, L. R. Wallenberg, L. Samuelson, and W. Seifert, *Adv. Funct. Mater.* **15**, 1603 (2005).
- ⁸S. A. Dayeh, E. T. Yu, and D. Wang, *Nano Lett.* **7**, 2486 (2007).
- ⁹E. Stern, G. Cheng, E. Cimpoiu, R. Klie, S. Guthrie, J. Klemic, I. Kretzschmar, E. Steinlauf, D. T.-Evans, E. Broomfield, J. Hyland, R. Koudelka, T. Boone, M. Young, A. Sanders, R. Munden, T. Lee, D. Routenberg, and M. A. Reed, *Nanotechnology* **16**, 2941 (2005).
- ¹⁰A. Motayed, M. Vaudin, A. V. Davydov, J. Melngailis, M. He, and S. N. Mohammad, *Appl. Phys. Lett.* **90**, 043104 (2007).
- ¹¹J.-R. Kim, B.-K. Kim, I. J. Lee, J.-J. Kim, J. Kim, S. C. Lyu, and C. J. Lee, *Phys. Rev. B* **69**, 233303 (2004).
- ¹²C. Y. Nam, D. Tham, and J. E. Fischer, *Nano Lett.* **5**, 2029 (2005).
- ¹³C. Thelander, M. T. Björk, M. W. Larsson, A. E. Hansen, L. R. Wallenberg, and L. Samuelson, *Solid State Commun.* **131**, 573 (2004).
- ¹⁴J. Salfi, U. Philipose, S. Aouba, S. V. Nair, and H. E. Ruda, *Appl. Phys. Lett.* **90**, 032104 (2007).
- ¹⁵M. He, I. Minus, P. Zhou, S. N. Mohammed, J. B. Halpern, R. Jacobs, W. L. Sarney, L. Salamanca-Riba, and R. D. Vispute, *Appl. Phys. Lett.* **77**, 3731 (2000).
- ¹⁶A. Motayed, R. Bathe, M. C. Wood, O. S. Diouf, R. D. Vispute, and S. Noor Mohammad, *J. Appl. Phys.* **93**, 1087 (2003).
- ¹⁷Y. Huang, X. Duan, Y. Cui, and C. M. Lieber, *Nano Lett.* **2**, 101 (2002).
- ¹⁸J.-R. Kim, H. M. So, J. W. Park, J.-J. Kim, J. Kim, C. J. Lee, and S. C. Lyu, *Appl. Phys. Lett.* **80**, 3548 (2002).
- ¹⁹H.-Y. Cha, H. Wu, M. Chandrashekar, Y. C. Choi, S. Chae, G. Koley, and M. G. Spencer, *Nanotechnology* **17**, 1264 (2006).
- ²⁰C.-Y. Chang, G.-C. Chi, W.-M. Wang, L.-C. Chen, K.-H. Chen, F. Ren, and S. J. Pearton, *J. Electron. Mater.* **35**, 738 (2006).
- ²¹B. S. Simpkins, P. E. Pehrsson, and A. R. Laracuate, *Appl. Phys. Lett.* **88**, 072111 (2006).
- ²²C. Xu, J. Chun, K. Rho, D. E. Kim, B. J. Kim, S. Yoon, S.-E. Han, and J.-J. Kim, *J. Appl. Phys.* **99**, 064312 (2006).
- ²³J. Zolper, R. G. Wilson, S. J. Pearton, and R. A. Stall, *Appl. Phys. Lett.* **68**, 1945 (1996).
- ²⁴M. E. Levinstein, S. L. Rumyantsev, and M. S. Shur, *Properties of Advanced Semiconductor Materials: GaN, AlN, InN, BN, SiC, SiGe* (Wiley, New York, USA, 2001), p. 8.
- ²⁵H. Morkoç, *Nitride Semiconductors and Devices* (Springer-Verlag, Berlin, 1999), p. 240.
- ²⁶D. C. Look, *Electrical Characterization of GaAs Materials and Devices* (Wiley, New York, USA, 1989), pp. 77–78.
- ²⁷G. L. Pearson and J. Bardeen, *Phys. Rev.* **75**, 865 (1949).
- ²⁸N. F. Mott, *Rev. Mod. Phys.* **40**, 677 (1968).